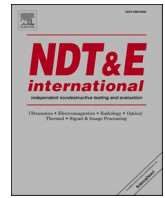| Title	In situ measurement of ultrasonic behavior during lap spot welding with laser ultrasonic method
Author(s)	Nomura, Kazufumi; Deno, Soshi; Matsuida, Taketo et al.
Citation	NDT and E International. 130 p.102662
Issue Date	2022-09
oaire:version	VoR
URL	https://hdl.handle.net/11094/88481
rights	This article is licensed under a Creative Commons Attribution 4.0 International License.
Note	

In situ measurement of ultrasonic behavior during lap spot welding with laser ultrasonic method

Kazufumi Nomura [*], Soshi Deno, Taketo Matsuida, Satoshi Otaki, Satoru Asai

Graduate School of Engineering, Osaka University, Japan

ARTICLE INFO

ABSTRACT

Understanding the joining process in real time during welding can help improve welding quality, reliability, and manufacturing process efficiency. For this purpose, a laser ultrasonic method that can detect in situ welding quality without contact during welding would be useful. However, the behaviors of ultrasonic propagation as well as melting and joining with increasing temperature remain unclear. Therefore, this study aimed to experimentally investigate the in-process ultrasonic behavior when using the laser ultrasonic method. Lapped tungsten inert gas (TIG) arc spot welding was used for the ultrasonic measurements, wherein the ignition of the TIG arc from the specimen's top surface and laser irradiation for the ultrasonic measurement from the bottom surface occur simultaneously. In this welding, the melting width at the interface of the lapped plates is an important parameter. We investigated the type of ultrasonics used to measure the melting width and examined whether the melting behavior during welding could be experimentally captured. The results show that the ultrasonic velocity decreases as the temperature increases. The echo from the interface between the plates disappears, and the echo from the top surface appears. The disappearance and appearance of each echo facilitate the understanding of the melting behavior during welding.

1. Introduction

Welding technology is used in various fields of the manufacturing industry and is an indispensable technology in manufacturing. However, many cases of destruction originate from welded joints, and high reliability is of utmost importance. Currently, non-destructive inspection is widely used after welding to guarantee welding quality. However, a significant backtracking process may occur if a defect is detected during inspection, which is time-consuming and expensive. Therefore, there is an increasing demand for in-process monitoring that detects the presence or absence of welding defects during welding. As the object becomes very hot during welding, it is necessary to apply an inspection method that is measurable even in severe environments. Appearance measurement with a visual camera and temperature measurement with thermography are non-contact methods and are often used as in-process monitoring methods [1,2], including additive manufacturing [3]. However, they are restricted to external information. It is necessary to find the correlation between external and internal information to obtain internal information. This correlation is an indirect connection, but it is often inapplicable when the conditions change. For example, our recent study estimated the depth of invisible internal penetration by machine learning from molten pool monitoring [4]; however, it is an indirect approach that is not based on principles of physics. Currently, only radiographic testing (RT) or ultrasonic testing (UT) is applicable for direct measurement of internal information. X-ray methods [5,6], airborne ultrasonic methods [7], electromagnetic ultrasonic methods [8], and laser ultrasonic methods [9,10] are considered to be useful for obtaining internal information on welds as a non-contact method in a high-temperature environment. The use of X-rays requires a large-scale device, and it is not easy to apply to thick steel materials. Furthermore, its application has many problems, such as the need for radiation safety management. Although airborne ultrasonic methods and electromagnetic ultrasonic methods can measure without any contact with an object, they must be set very close to the object, and the signal-to-noise ratio (SNR) is generally low. Therefore, it is difficult to apply them in an environment such as welding. Here, we focused on the laser ultrasonic method, which generates and detects ultrasonics remotely. The laser ultrasonic method can excite ultrasonics by pulse laser irradiation and receive them on the target surface using a laser interferometer. Because a laser is used as a probe, non-contact measurement can be performed

---

remotely to apply it even under high-temperature conditions such as welding. In addition, the laser ultrasonic method has the following advantages compared to conventional ultrasonic testing with a transducer: (1) it is possible to excite high-frequency ultrasonic waves of several tens of MHz in a wide band, so an improved spatial resolution of ultrasonic detection; (2) because of its small beam diameter, it is also applicable to narrow areas; (3) the measurement system can be scanned at high speed [10,11].

Currently, laser ultrasonic methods are used in various studies, such as defect detection [12–16], plate thickness measurement [17], and material property evaluation [18–21]. As an example of applying the laser ultrasonic method during welding, Yamamoto et al. reported the detection of welding defects during butt welding of thick Cr–Mo–V steel pipes and compared the dimensions of the defects with conventional ultrasonic tests [22]. Nomura et al. detected welding defects, such as lack of penetration and solidification cracks, during gas metal arc welding of single-bevel groove joints [23,24]. They also detected changes in penetration depth when welding conditions changed [24]. In recent years, there have been reports of real-time monitoring of welding quality using laser ultrasonic methods during welding, demonstrating their usefulness. Additive manufacturing is also a technology that utilizes the phenomenon of melting and joining, and the development of its non-destructive testing (NDT) technique is required [3]. The laser ultrasonic method has attracted attention because of the possibility of its application to inspections for each pass [25,26]. However, few studies have been conducted on the process involving the melted area. Hence, studies have not yet clarified how ultrasonic waves propagate through the melting and joining process. From the point of view of the high-temperature field, there are many studies on the measurement of ultrasonic velocity [19,27–31]. It is widely known that the ultrasonic velocity generally decreases as the temperature increases. The detection of the solid-liquid interface in Al has been reported by Burhan et al. as an example of solidification behavior [32]; however, the subject is not a joining phenomenon. Welding is a phenomenon in which multiple materials fuse as the temperature increases, and there are a few reports on the ultrasonic behavior during the phenomenon of joining. When the ultrasonic propagation behavior during welding can be clarified, and the melting and joining phenomenon can be grasped in real-time, it will be beneficial for controlling the welding quality and understanding the phenomenon.

Therefore, we aimed to grasp the melting and joining phenomenon using the laser ultrasonic method to clarify the ultrasonic behavior during welding with temperature-rise. In this study, we conducted lap arc spot welding as one of the systems where such phenomena occur [33]. The internal joint diameter of lap arc spot welding is important to ensure joint strength. However, the visible processed diameter and the internal joint diameter generally do not match, and in some cases, the joint may be misaligned and deviated [34,35]. Therefore, there is a demand practically to measure the internal joint diameter. Furthermore, in-process measurement is useful to prevent insufficient penetration and burn-through. In the lap arc spot welding by the tungsten inert gas (TIG) arc, the upper plate firstly melts, and the interface between the upper and lower plates gradually melts, and two plates are finally joined. We investigated what kind of wave should be used for the laser ultrasonic method to capture this phenomenon. TIG arc spot welding is often discussed to study fundamental issues [36,37]. In addition, recently, a dissimilar material welding method using an intermediate layer [38] and a specific element [39] has been reported. Therefore, there is also a demand for experimentally measuring the melting phenomenon of the arc spot welding method. This study clarifies the basic phenomenon measured when diagnosing the state of invisible internal joints in such spot-shaped lap welding with ultrasonics.

This paper shows the measurement result where the plate thickness of the lap specimen was relatively thick after describing the experimental equipment configuration, measurement system, and measurement conditions. Next, we show the measurements made on thin lap plates, which are rather difficult to apply to ultrasonic methods.

2. Methods

2.1. Experimental setup

Fig. 1 shows a schematic of the experimental setup. The specimen consisted of two stacked steel plates. The TIG arc was ignited at a fixed point from the specimen's top surface to form a molten pool during welding. At the same time, the ultrasonic measurement lasers, which were generation and detection lasers, were irradiated at the bottom surface. Tables 1 and 2 show the specifications of the generation and detection lasers used in this experiment, respectively. The generation laser was a pulsed Nd:YAG laser with a wavelength of 1064 nm (Litron Lasers, Nano L90-100). There are two types of ultrasonic excitation modes excited by a laser: thermoelastic and ablation [6]. In this study, the pulse energy and the spot diameter were selected where the ultrasonic waves were excited in the ablation region: the pulse energy was 30 mJ, the pulse width was 8 ns, and the spot diameter at the irradiation point was approximately 1.5 mm. The detection laser consisted of an Nd:YAG laser with a wavelength of 532 nm and a laser interferometer based on the Michelson interferometer by multichannel random orthogonal interferometry (Bossa Nova, Quartet-1500) [40]. The detection laser was irradiated at one point and orthogonal to the measurement surface. The measured signal intensity was proportional to the detection sensitivity of the detection laser device. The detection sensitivity depends on the reference light intensity and decreases because of the following
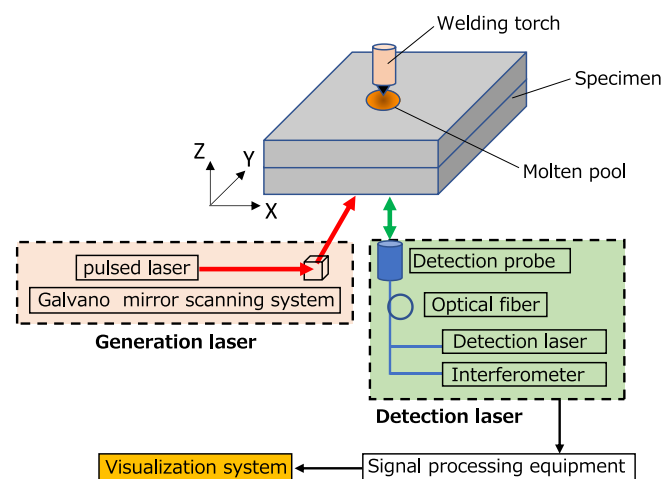

Fig. 1. Schematic of the experimental setup.

Table 1
Specification of the generation laser.

Laser	Nd:YAG
Wavelength	1064 nm
Repetition rate	100 Hz
Energy	30 mJ
Pulse width	8 ns
Beam diameter	1.5 mm

Table 2
Specification of the detection laser.

Laser	Nd:YAG
Wavelength	532 nm
Laser power	1 W
Detection range	100 kHz–50 MHz

(a) Thick plate condition (2 mm + 6 mm)   (b) Thin plate condition (2 mm + 2 mm)

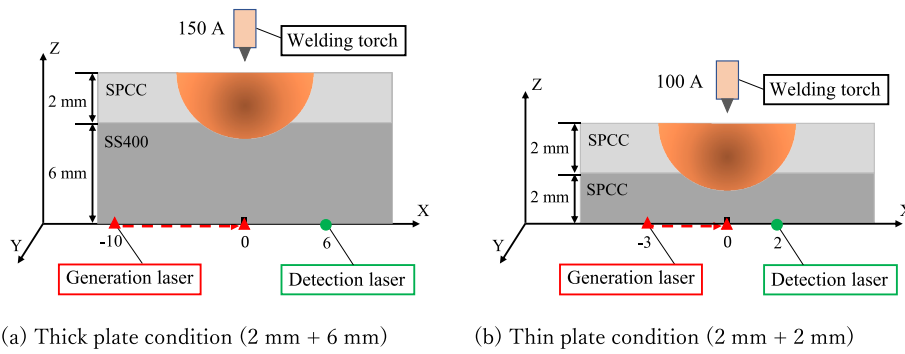**Fig. 2.** Schematic of the measurement conditions.

Table 3
Ultrasonic velocities of samples at room temperature.

	SS400	SPCC
Longitudinal wave [m/s]	5920	5970
Transverse wave [m/s]	3200	3240

factors: the distance between the probe and the target deviates from the focal position, the irradiation angle is tilted, and the reflectance of the target surface is low. In this study, the position and angle of the probe were adjusted to maximize the detection sensitivity. The generation laser was irradiated at multiple points for a set length with a Galvano mirror scanner, and the procedure was repeated during welding. As a result, we continuously acquired the B-scans, whose horizontal axis is the generation position and the vertical axis is the ultrasonic propagation time and evaluated their time change. The acquired signal was not averaged, and a frequency filter was applied to cut below 3 MHz and above 10 MHz for noise reduction.

2.2. Measurement conditions

The specimen consisted of two stacked steel plates, and the four corners were clamped to bring them into close contact with each other. A schematic of the experiment is presented in Fig. 2. We evaluated the two types of specimens. One was the thick plate condition, where the thicknesses of the upper and lower plates were 2 and 6 mm, respectively. The other was the thin plate condition, where the upper and lower plates were 2 mm thick. The lasers were irradiated to the bottom surface of the lower plate to measure the ultrasonic waves. The ultrasonic behavior can be relatively easier to identify for the thick plate condition than the thin plate type because the thick plate condition is less affected by multiple reflections. However, in typical lap plate joining, the same thin plates are used in many cases. Therefore, we attempted to measure these

two conditions.

SPCC was used for the 2 mm thick plate, and SS400 was used for the 6 mm thick plate. The size of the XY surface of both plates was 200×80 mm. The use of two types of steel was simply a matter of the standard plate thickness availability. Table 3 presents the results of the ultrasonic velocity measurement in this study. This results from irradiating the generation laser from one side of the plate, arranging the detection laser on the opposite side, and measuring the ultrasonic at room temperature while changing the distance between the generation and detection points. No significant differences in velocities were observed. Accurate ultrasonic velocity measurement in a high-temperature field requires a uniform temperature distribution, which was not conducted in this study. It is generally known that the ultrasonic velocity decreases as the temperature increases.

The laser irradiation conditions in the thick plates (see Fig. 2 (a)) were as follows: where X = 0 mm was set below the welding target position, the detection point was one point of X = 6 mm, and the generation laser was scanned from X = −10 to 0 mm with a pitch of 0.2 mm, for a total of 51 points. As the repetition rate of the generation laser was 100 Hz, it took 0.5 s to scan this generation range equally to obtain one B-scan. The signal was acquired at 100 MS/s and processed in real-time. For the thin plates (see Fig. 2 (b)), the laser irradiation conditions were as follows: the detection point was one point at X = 2 mm, the generation laser was scanned from X = −3 to 0 mm with a pitch of 0.2 mm, for a total of 16 points. For both the conditions, an offset distance of 3 mm was set between the generation and detection points in the Y direction. Therefore, the line by generation points was Y = 1.5 mm, and the detection point was Y = −1.5 mm, where Y = 0 mm was set below the welding target position. Due to this offset influence, the propagation distance is slightly longer than under the condition when the generation and detection points are lined up at Y = 0 mm. For example, when the distance between the generation and detection points is 12 mm in the X direction, and the reflection occurs at z = 6 mm, the propagation distance without offset is 16.9 mm. With an offset in the Y direction of 3 mm, the propagation distance changes 17.2 mm, which is 1.02 times the original. Although with larger distances, the offset effect becomes smaller, this study supposes that this deviation has no significant effect on the measurements and evaluations.

The heat source, the TIG arc, ignited on the top surface of the upper plate. The welding conditions were as follows: the shielding gas was Ar with a flow rate of 15 L/min, an arc length of 3 mm, and a tungsten electrode diameter of 3.2 mm. The welding current and welding time were selected to melt the interface between two plates, but no burn-through occurred. The parameters were 150 A and 48 s under the thick plate condition, 100 A and 30 s under the thin plate condition.
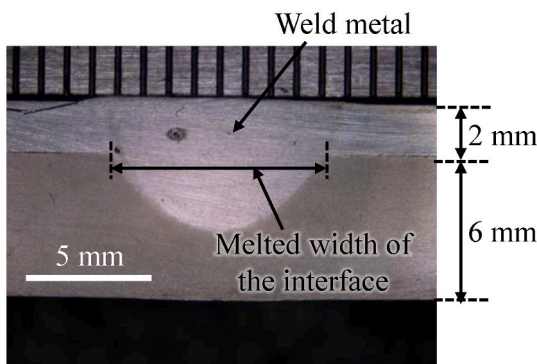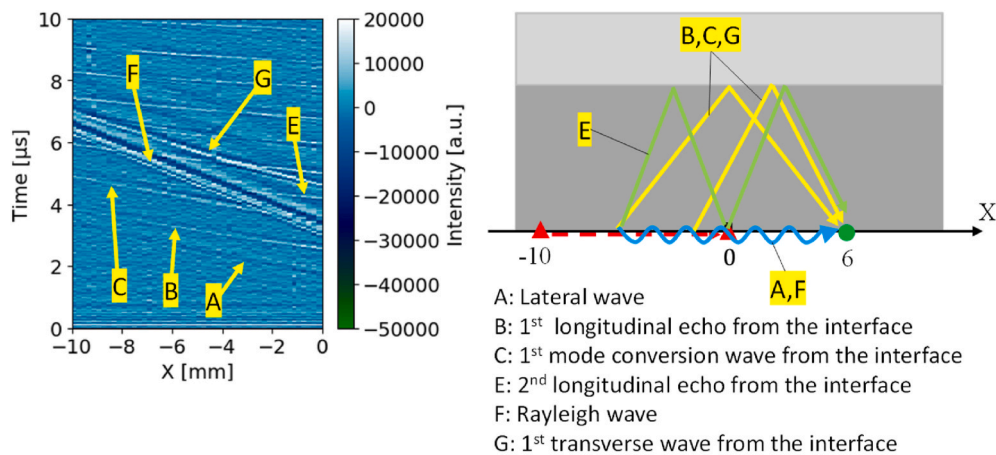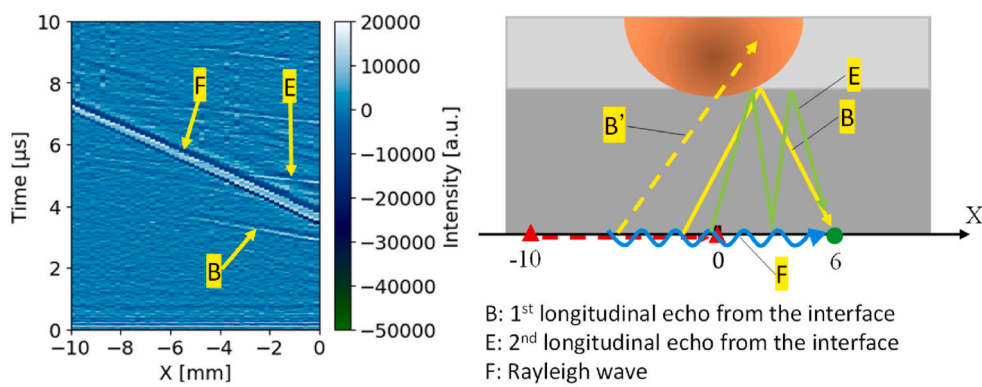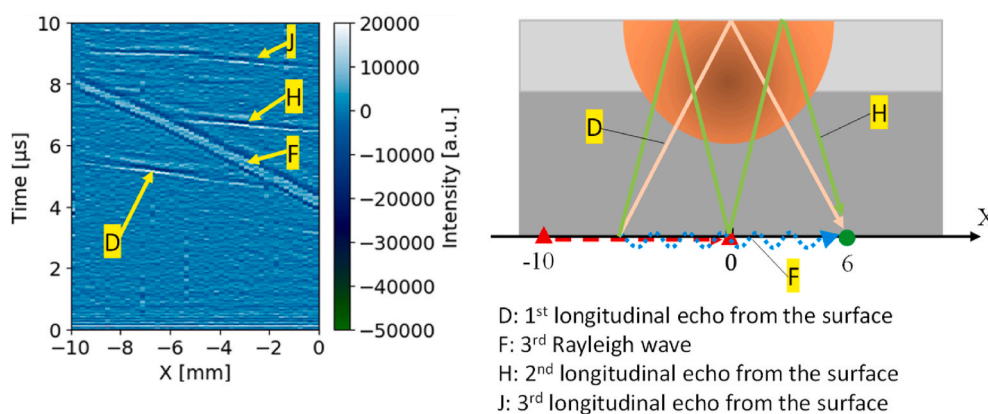

Fig. 3. Cross-sectional macro after the welding time of 48 s under the thick plate condition.

A: Lateral wave
B: 1st longitudinal echo from the interface
C: 1st mode conversion wave from the interface
E: 2nd longitudinal echo from the interface
F: Rayleigh wave
G: 1st transverse wave from the interface

(a) Immediately after arc ignition

B: 1st longitudinal echo from the interface
E: 2nd longitudinal echo from the interface
F: Rayleigh wave

(b) 17 s after welding starts

D: 1st longitudinal echo from the surface
F: 3rd Rayleigh wave
H: 2nd longitudinal echo from the surface
J: 3rd longitudinal echo from the surface

(c) 34 s after welding starts

Fig. 4. Time variation of the B-scan during TIG arc spot welding in 2 mm and 6 mm plates.

3. Results

3.1. Thick plate condition

For observing the melting and joining phenomenon during TIG spot welding using laser ultrasonic, it is necessary to consider the effective arrangement of laser irradiation and the type of wave that can be used to make it possible. In this section, in-process measurement by laser ultrasonic was performed for the specimen using relatively thick plates, which are easy to identify without superimposing each excited ultrasonic wave by multiple reflections.

The measurement conditions are shown in Fig. 2 (a). Fig. 3 shows a cross-sectional macro 48 s after the start of welding. This cross-sectional macro shows that the interface was fused at a width of 8 mm and melted at a depth of approximately 5 mm due to the 48 s heating by the TIG arc spot welding.
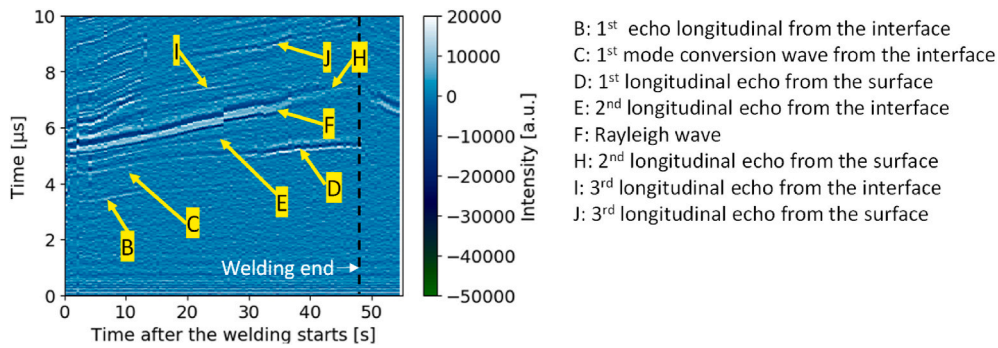
Fig. 5. Time variation of the A-scope obtained at one generation point of X = −6 mm.
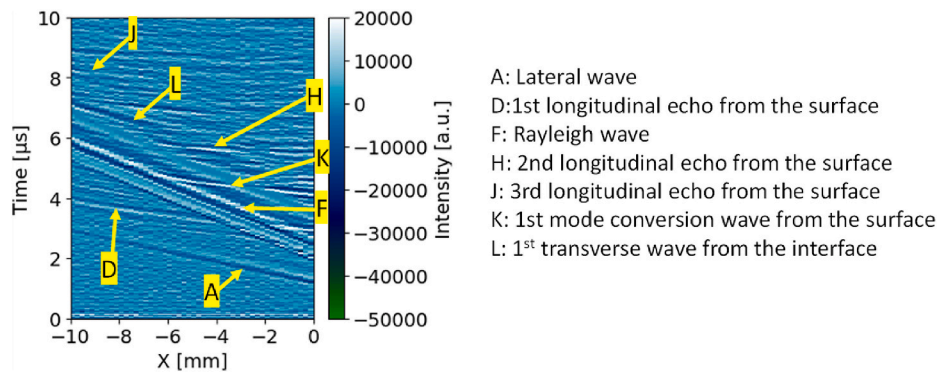

Fig. 6. Post-processing of the B-scan at room temperature.

Fig. 4 (a) to **(c)** show the B-scan at 0, 17, and 34 s after the arc ignition. In addition, the plots on the right show the supposed state of some ultrasonic propagation within the specimen varying with time. The various waves were observed; therefore, we assigned capital letters to each wave to distinguish them commonly in the plots.

Fig. 4 (a) shows that the interface between the upper and lower plates did not melt at the start of welding. We can see the various waves over the entire generation range: surface waves such as lateral (A) and Rayleigh waves (F), longitudinal and transverse waves reflected once at the interface (1st longitudinal echo (B) and 1st transverse echo (G) from the interface), mode conversion wave reflected once at the interface (C), and the longitudinal wave reflected twice at the interface (2nd longitudinal echo from the interface (E)). These results are consistent with the arrival time converted from the longitudinal wave and transverse wave velocities at room temperature, respectively. The 1st longitudinal echo was weaker on the left side of the B-scan, but this was considered due to the directivity of the laser ultrasonic longitudinal wave in the ablation mode [6].

Fig. 4 (b) shows the change in each echo as welding progressed and the interface melted. The range in which the 1st longitudinal echo can be obtained is narrowed, and the signal is hardly seen on the left side of the B-scan. We assumed this was because the interface melted as shown in the corresponding illustration; thus, the waves became hard to reflect at the interface depending on the irradiation position. As welding progressed further, the longitudinal wave reflected once at the top surface of the upper plate (1st longitudinal echo from the surface (D)) appeared clearly in a wide range (Fig. 4 (c)). In addition, waves that reflected two (H) and three (J) times from the top surface were also observed. It is also shown that the signal intensity of the surface wave appears to be weakened. Moreover, Fig. 4 (b) and (c) show that bulk waves related to transverse waves were no longer observed. Because the transverse wave generally does not propagate through and is not reflected at the liquid, it is considered that a part of the interface melted. However, there should be a slight longitudinal wave reflection from the solid-liquid interface

[32,41]. This reflection was not visually recognized in this measurement, probably because of its very low signal intensity.

From the above results, we can propose using the intensity decline of the 1st echo from the interface (B) or the appearance of the 1st echo from the top surface (D) to capture the widening of the interfacial fusion width, that is, the joining phenomenon.

3.2. Monitoring at one generation point of thick plate condition

To clarify the time variation of ultrasonic propagation due to heating and melting of the interface by the TIG arc spot, we focused on the signal variation at a point X = −6 mm on behalf of the generation point where the 1st longitudinal echo from the top surface was obtained. The signals were picked up at X = −6 mm from each B-scan and laterally arranged in Fig. 5, where the welding time is on the horizontal axis and the ultrasonic propagation time is on the vertical axis. Because it takes 0.5 s to acquire one B-scan, the time resolution on the horizontal axis in Fig. 5 is also 0.5 s. The explanation in capital letters is the same as that in Fig. 4. As welding progressed and the temperature of the specimen increased, the ultrasonic velocities decreased, and the propagation time of the ultrasonic wave was delayed overall. The behavior of these waves changed discontinuously at 48 s because the specimen was rapidly cooled after the welding.

First, the 1st echo intensity from the interface (B) decreased as the welding progressed, as described in Section 3.2. Second, the 1st echo from the top surface (D) started appearing approximately 20 s after the welding commenced, and its intensity gradually increased. In Fig. 5, the mode conversion wave (C) and the echo from the top surface (D) appear to be connected to one signal; however, they are different waves. The arrival times were very close under these experimental conditions, but observing their time change in the B-scans enabled us to distinguish between these two waves. For example, we can see that the corresponding wave disappeared in Fig. 4 (b), which shows the transition state. Therefore, it can be inferred that these two waves have different
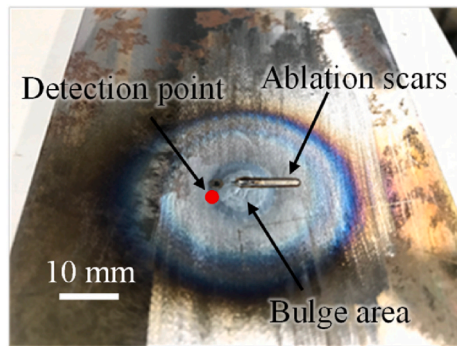
Fig. 7. The appearance of the bottom surface after the TIG arc spot welding under the thick plate condition.
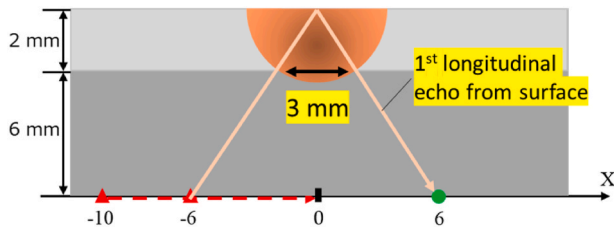

Fig. 8. Simple geometric calculation for detecting the 1st longitudinal echo from the top surface.

Fig. 9. Cross-sectional macro at 34 s after the welding starts.

Fig. 10. Cross-sectional macro after the welding time 30 s of thin plate condition.

origins. The 1st surface echo (D) intensity increased as the interfacial melting progressed, which is considered because melting and fusion broadened the gate-like area for the incoming and outgoing ultrasonic waves to the upper plate.

After the welding was completed, the arrival time of the 1st echo from the top surface (D) changed quickly from 5 μs to 4.5 μs as the temperature dropped. At the same time, the signal intensity also decreased significantly due to the decrease in the detection laser sensitivity. In this welding, the bottom surface of the specimen became red-hot and oxidized just below the welding target position. At 48 s after the welding started, the discoloration covered the detection point due to the expansion of the red-hot area. Changes in the detection surface significantly induced the detection sensitivity. For recovering the detection sensitivity, we post-processed the measurement by polishing the detection area of the specimen after the in-process measurement. The resulting B-scan is shown in Fig. 6. We can see that the 1st echo from the top surface (D) with sufficient intensity improves the detection sensitivity. The arrival time of this signal at X = −6 mm is approximately 3.5 μs, which matches the time obtained by a simple geometric calculation. On the other hand, the arrival time of this wave (D) at 50 s in Fig. 5 was approximately 4.5 μs, which is low but can be observed. This indicated that the specimen at 50 s was still hot for ultrasonic propagation. Furthermore, Fig. 6 shows that the waves related to the transverse wave were observed again, and the mode conversion wave reflected on the top surface (K) was observed for the first time, unlike displayed in Fig. 4 (b) and (c).

The arrival time of the Rayleigh wave (F) was suddenly delayed while focusing on it approximately 26 s after the start of the welding in Fig. 5. However, no such delay was observed in other waves as the heating specimen affected the bottom surface and induced a slight and partial bulge (see Fig. 7). Furthermore, the Rayleigh wave intensity gradually decreased from approximately 35 s after the start of welding. Because the intensity of the 1st echo from the top surface (D) remains high, it was suggested that the detection sensitivity did not induce a decrease in the Rayleigh wave intensity. If this happened due to the decline in detection sensitivity, the Rayleigh wave intensity should not increase after the welding, where the discoloration remained. This
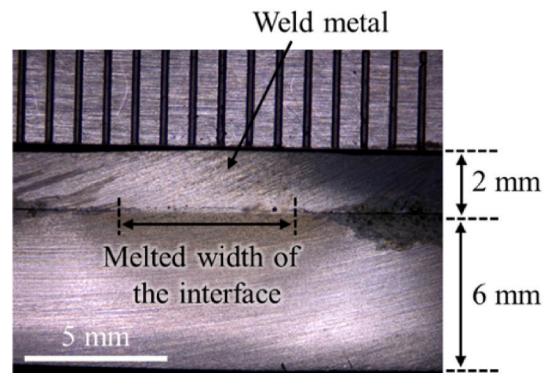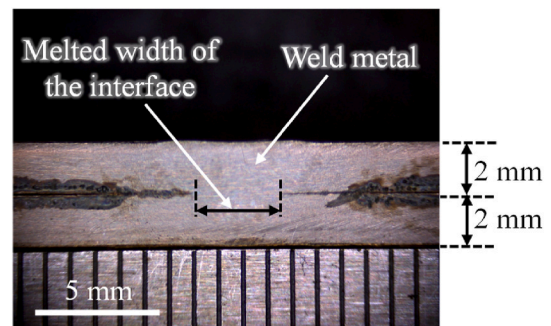
phenomenon is discussed in Section 3.4.

Using the results, we estimated the width of the melting interface on a trial basis. According to the simple geometric relationship shown in Fig. 8, if the 1st echo from the top surface is obtained by the generation at X = −6 mm, with at least 3 mm openings, the interfacial melting should exist. Therefore, after the welding started, we stopped it at 34 s and observed its cross-sectional macro (Fig. 9). The 1st echo from the top surface was sufficiently observed. The melted width exceeded 3 mm and was observed to be approximately 6 mm. Therefore, it can be said that to capture the melting phenomenon of lapped spot welding, an echo from the surface with relatively high intensity is suitable. Strictly speaking, a correlation investigation between the measured signal intensity and the melted width is required; however, laser ultrasonic measurement such as the above method can guarantee the melted width by using the appearance of 1st echo from the top surface. More detailed experiments and discussions are required for rigorous sizing.
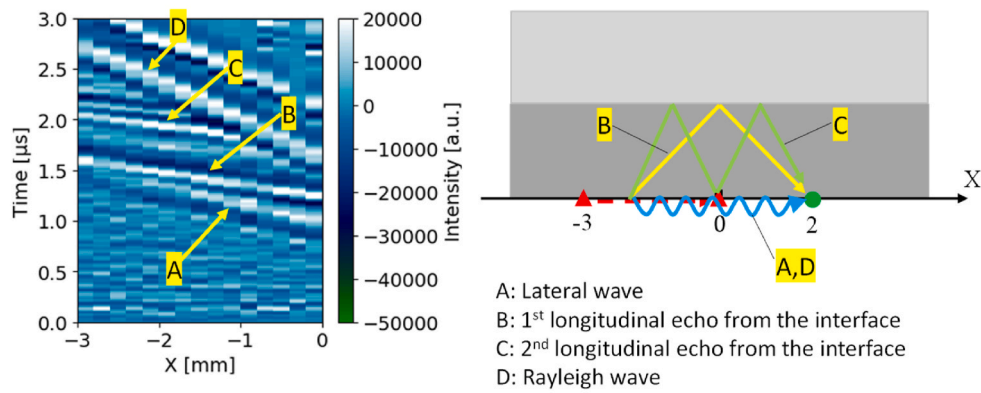
3.3. Thin plate condition

The previous subsections show that we can capture the melting and joining phenomenon using appropriate echoes in laser ultrasonic measurements. The specimen was a combination of a 2 mm upper plate and a 6 mm lower plate. Because the lower plate was thick, the ultrasonic waves were relatively easy to distinguish. However, in typical lap plate joining, plates of the same thickness are generally used. This section examines the possibility that our measurement could be applied to thin plate specimens with a thickness of 2 mm for both the upper and lower SPCC plates. The experimental conditions are shown in Fig. 2 (b). The welding time was 30 s when the interface between the plates melted, and no burn-through occurred. Fig. 10 shows a cross-sectional macro 30 s after the start of welding. This cross-sectional macro shows that the interface was fused at a width of approximately 3 mm.
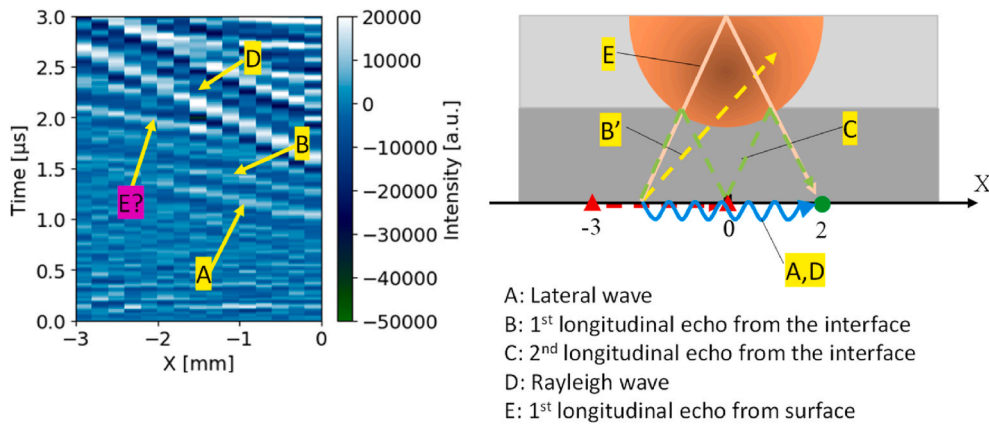
Fig. 11 (a) to (c) show the B-scans of 0 s, 20 s, and 30 s after the arc ignition following a supposed state of ultrasonic propagation within the
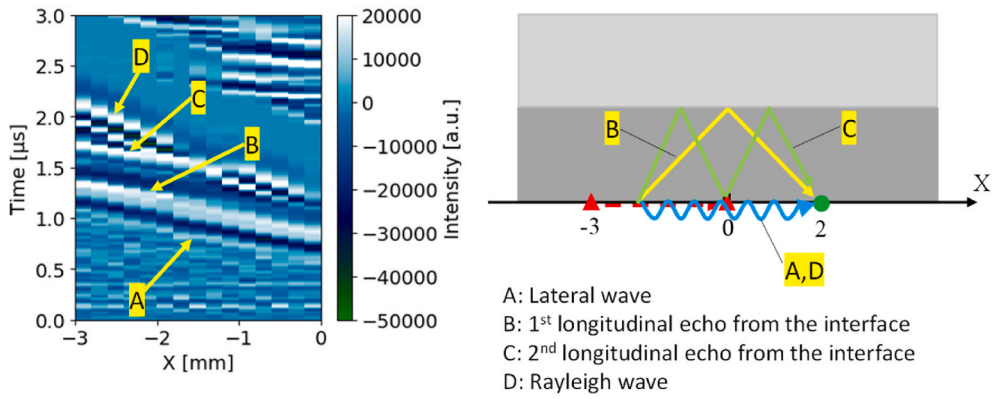
(a) Immediately after arc ignition

(b) 20 s after welding starts

(c) 30 s after welding starts

Fig. 11. Time variation of the B-scan during TIG arc spot welding in thin plate condition.

specimen at each time. We confirmed that the interface was not melted after 20 s but the joining was achieved in 30 s (Fig. 10) by multiple post-process observations after welding. It was shown that the melting and joining occurred between 20 and 30 s. In Fig. 11 (a) immediately after arc ignition, the Rayleigh wave (D), the lateral wave (A), and the 1st (B) and 2nd (C) longitudinal echoes emerge from the interface. These results are consistent with the arrival time converted from the ultrasonic velocities at room temperature. From Fig. 11 (b), the same waves displayed

in Fig. 11 (a) were still measured with a delayed time, although the interface was not melted. Because the plate was thinner, it was expected that the lower plate would become hot enough to slow the ultrasonic waves before the interface melted. Fig. 11 (c), When the interface was melted by approximately 3 mm, it showed that the intensity of the 1st echo from the interface (B) decreased less than earlier, which was similar to that of the thick condition. If the phenomenon is the same as the thick condition, the echo from the top surface (E) should be obtained

subsequently. However, because the simple geometric calculation shows that the arrival time of the 1st echo from the top surface (E) and the 2nd echo from the interface (C) become the same under this irradiation condition, the waves cannot be distinguished. This always occurs when the upper and lower plate thicknesses are the same; thus, it is difficult to regard the appearance of the echo from the top surface (E) as a sign of melting. In a precise sense, the echo from the top surface should be slower than the echo from the interface because the former wave propagates through the upper plate, which has a higher temperature region. However, there was no visible difference in the propagation delay of the ultrasonic waves.

4. Discussion

Depending on the thickness of the plate, there is some useable ultrasonic information to capture the phenomenon of joining. In the results of the thick plate condition, the decline in the intensity of the 1st echo from the interface or the appearance of the 1st echo from the top surface is useful. For thin plates of the same thickness, it is possible to use the intensity decrease of the 1st echo from the interface. However, because the arrival times of the 1st echo at the interface and the lateral wave are very close, to evaluate the reduction in the intensity quantitatively and to guarantee the melted interface length are more difficult than the thick plate condition.

On the other hand, changes in the behavior of the surface waves were also observed during the in-process. As mentioned in Section 3.2, Fig. 5 shows that the Rayleigh wave intensity decreased significantly after approximately 35 s from the start of welding. The aiming position of this welding was at X = 0 mm and Y = 0 mm, and the discolored area expanded from this center at the bottom surface. When the laser ultrasonic measurement set the generation and detection points as X = −6 mm and 6 mm, the Rayleigh wave propagated through the red-hot center, as shown in Fig. 12. We considered that the temperature rise of the propagation path was the cause of the signal intensity decline. Thus, we measured the temperature change of the bottom surface non-contactly during welding time using thermography. A blackbody spray was used to avoid the emissivity problem for thermographic measurements. Fig. 13 shows the time variation of the peak-to-peak values of the Rayleigh wave intensity and central temperature. This figure shows that the Rayleigh wave intensity decreased significantly between the welding time of 30 s and 35 s, and the corresponding temperature in the central area was approximately 1000 °C (Fig. 13). It was suggested that Rayleigh waves might be significantly attenuated by propagating at approximately 1000 °C. We have incorporated the change in detection sensitivity to this figure to show that this attenuation was not due to the decrease in detection sensitivity. Rayleigh waves are elastic surface waves combined with longitudinal and transverse waves, and the liquid does not transmit transverse waves. It is supposed that as the bottom side is softened enough to deform the surface, the propagation of the transverse waves is impeded. Consequently, the surface wave is significantly attenuated. Regarding the attenuation of bulk waves, Scruby et al. reported that rapid attenuation was observed at 1000 °C [28]. Because in
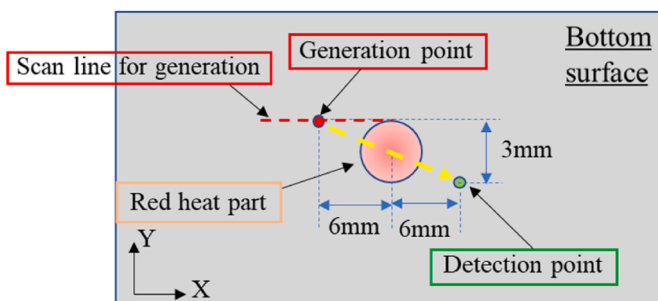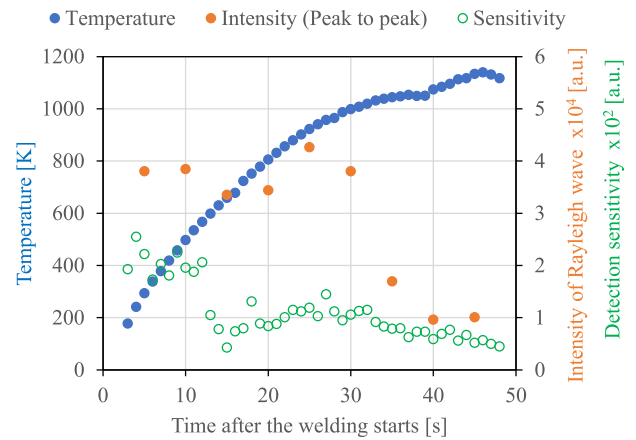

Fig. 13. Time variation of the peak-to-peak value of the Rayleigh wave intensity and the central temperature.

their measurement, the material is sandwiched between the generation and detection lasers, it did not directly indicate the attenuation of the surface wave intensity. However, this was considered to be closely related to our results. Investigation of the complex behavior of the surface wave at a high-temperature state is expected to be discussed further.

5. Conclusions

This study experimented with laser ultrasonic measurement for lapped TIG arc spot welding composed of two steel plates. The TIG arc was ignited on the surface of the upper plate. The scanned multi-point generation laser and one-point detection laser were used to irradiate the bottom surface of the lower plate. We aimed to capture the fusion and joining phenomenon using laser ultrasonic and clarify the ultrasonic behavior during such a high-temperature field in-process.

When the upper plate was 2 mm, and the lower plate was 6 mm of the specimen, we could capture the melting phenomenon at the interface using the decrease in the intensity of the 1st longitudinal echo from the interface or the appearance of the 1st longitudinal echo from the top surface. Furthermore, it showed that the Rayleigh wave, one of the surface waves, is significantly attenuated when it propagates above approximately 1000 °C.

In a thinner specimen with the upper and lower plates set to 2 mm, the decrease in the intensity of the 1st longitudinal echo from the interface was functional to capture the melting phenomenon. However, we were unable to recognize the 1st echo from the top surface because the arrival times of the 2nd echo from the interface and the lateral wave were close to each other. Therefore, it is difficult to make a quantitative judgment when the specimen is a thick plate.

Fig. 12. Propagation path of the surface wave at the bottom surface.

Declaration of competing interest

The authors declare that they have no known competing financial interests or personal relationships that could have appeared to influence the work reported in this paper.

References

[1] Cheng Y, Yu R, Zhou Q, Chen H, Yuan W, Zhang Y-M. Real-time sensing of gas metal arc welding process – a literature review and analysis. J Manuf Process 2021; 70:452–69.

[2] Asai S, Tanaka M, Yamane S, Miyasaka F, Shigeta M, Nomura K, Ogino Y. Recent progress of welding and joining engineering. J Jpn Weld Soc 2020;89(5):322–35 [in Japanese)].

[3] Lopez A, Bacelar R, Pires I, Santos TG, Sousa JP, Quintino L. Non-destructive testing application of radiography and ultrasound for wire and arc additive manufacturing. Addit Manuf 2018;21:298–306.

[4] Nomura K, Fukushima K, Matsumura T, Asai S. Burn-through prediction and weld depth estimation by deep learning model monitoring the molten pool in gas metal arc welding with gap fluctuation. J Manuf Process 2021;61:590–600.

[5] Morisada Y, Fujii H, Kawahito Y, Nakata K, Tanaka M. Three-dimensional visualization of material flow during friction stir welding by two pairs of X-ray transmission systems. Scripta Mater 2011;65(12):1085–8.

[6] Hanke R, Fuchs T, Uhlmann N. X-ray based methods for non-destructive testing and material characterization. Nucl Instrum Methods Phys Res Sect A Accel Spectrom Detect Equip 2008;591(1):14–8.

[7] Gan TH, Hutchins DA. Air-coupled ultrasonic tomographic imaging of high-temperature flames. IEEE Trans Ultrason Ferroelectrics Freq Control 2003;50(9): 1214–8.

[8] Hernandez-Valle F, Dixon S. Initial tests for designing a high temperature EMAT with pulsed electromagnet. NDT E Int 2010;43(2):171–5.

[9] Hutchins DA. Ultrasonic generation by pulsed lasers. Phys Acoust 1988;18:21–123.

[10] Scruby CB, Drain LE. Laser ultrasonic, techniques and applications. Bristol: Adam Hilger; 1990.

[11] Krishnaswamy S. Theory and applications of laser-ultrasonic techniques. In: Ultrasonic nondestructive evaluation - engineering and biological material characterization; 2004. p. 435–94.

[12] An YK, Park B, Sohn H. Complete noncontact laser ultrasonic imaging for automated crack visualization in a plate. Smart Mater Struct 2013;22(2):025022.

[13] Choquet M, Heon R, Padioleau C, Bouchard P, Neron C, Monchalin JP. Laser-ultrasonic inspection of the composite structure of an aircraft in a maintenance hangar. Rev Prog Quant Nondestr Eval 1995;14:545–52.

[14] Liu P, Sohn H, Park B. Baseline-free damage visualization using noncontact laser nonlinear ultrasonics and state space geometrical changes. Smart Mater Struct 2015;24(6):065036.

[15] Spytek J, Sujdak AZ, Dziedziech K, Pieczonka L, Pelivanov I, Ambrozinski L. Evaluation of disbonds at various interfaces of adhesively bonded aluminum plates using all-optical excitation and detection of zero-group velocity Lamb waves. NDT E Int 2020;112:102249.

[16] Pei C, Yi D, Liu T, Kou X, Chen Z. Fully noncontact measurement of inner cracks in thick specimen with fiber-phased-array laser ultrasonic technique. NDT E Int 2020; 113:102273.

[17] Fuse N, Kaneshige K, Watanabe H. Development of thickness measurement system for hot steel with laser-ultrasonic wave technology. Mater Trans 2014;55:1011–6.

[18] Sarkar S, Moreau A, Militzer M, Poole WJ. Evolution of austenite recrystallization and grain growth using laser ultrasonics. Metall Mater Trans A 2008;39:897–907.

[19] Zamiri S, Reitinger B, grün H, Roither J, Bauer S, Burgholzer P. Laser ultrasonic velocity measurement for phase transformation investigation in titanium alloy. IEEE Int Ultrason Symp 2013:683–6.

[20] Aussel JD, Monchalin JP. Precision laser-ultrasonic velocity measurement and elastic constant determination. Ultrasonics 1989;27:165–77.

[21] Karabutov A, Devichensky A, Ivochkin A, Lyamshev M, Pelivanov I, Rohadgi U, Solomatin V, Subudhi M. Laser ultrasonic diagnostics of residual stress. Ultrasonics 2008;48(6–7):631–5.

[22] Yamamoto S, Hoshi T, Miura T, Semboshi J, Ochiai M, Fujita Y, Ogawa T, Asai S. Defect detection in thick weld structure using welding in-process laser ultrasonic testing system. Mater Trans 2014;55:998–1002.

[23] Nomura K, Otaki S, Kita R, Asai S. In-situ detection of weld defect during the welding process by laser ultrasonic technique. Proceedings of Meetings on Acoustics 2020;38(1):030016.

[24] Otaki S, Matsuida T, Nomura K, Imura F, Kita R, Asai S. In-situ measurement of weld quality during MAG welding using laser ultrasonic. Weld Int 2019;33:10–2.

[25] Patel R, Hirsch M, Dryburgh P, Pieris D, Yeboah SA, Smith R, Light R, Sharples S, Clare A, Clark M. Imaging material texture of as-deposited selective laser melted parts using spatially resolved acoustic spectroscopy. Appl Sci 2018;8:1991.

[26] Zeng Y, Wang X, Qin X, Hua L, Xu M. Laser ultrasonic inspection of a wire + arc additive manufactured (WAAM) sample with artificial defects. Ultrasonics 2021; 110:106273. Pubmed.

[27] Wadley HNG, Norton SJ, Mauer F, Droney B. Ultrasonic measurement of internal temperature distribution. Phil Trans Roy Soc Lond A 1986;320:341–61.

[28] Scruby CB, Moss BC. Non-contact ultrasonic measurements on steel at elevated temperatures. NDT E Int 1993;26(4):177–88.

[29] Dewhurst RJ, Edwards C, Mckie ADW, Palmer SB. A remote laser system for ultrasonic velocity measurement at high temperatures. J Appl Phys 1998;63:1225.

[30] Dubouis M, Moreau A, Bussiere JF. Ultrasonic velocity measurements during phase transformations in steels using laser ultrasonics. J Appl Phys 2001;89(11): 6487–95.

[31] Burgess K, Prakapenka V, Hellebrand E, Zinin PV. Elastic characterization of platinum/rhodium alloy at high temperature by combined laser heating and laser ultrasonic techniques. Ultrasonics 2014;54:963–6.

[32] Burhan D, Ihara I, Seda Y. In situ observations of solidification and melting of aluminum using ultrasonic waveguide sensor. Mater Trans 2005;46(9):2107–13.

[33] Cevik A, Kutuk MA, Erklig A, Guzelbey IH. Neural network modeling of arc spot welding. J Mater Process Technol 2008;202(1–3):137–44.

[34] Eda S, Ogino Y, Asai S, Hirata Y. Numerical study of the influence of gap between plates on weld pool formation in arc spot welding process. Weld World 2018;62: 1021–30.

[35] Furusako S, Matsui S, Zeniya T, Wakabayashi C, Okuda T, Shimada N, Fujimoto H. Assembly technology of welding and joining for ultra-high strength steel sheets for automobiles – spot welding. Nippon Steel Tech Rep 2019;122:65–75.

[36] De A. Spot welding. Sci Technol Weld Join 2008;13(3):213–4.

[37] Zhang W, Roy GG, Elmer JW, DebRoy T. Modeling of heat transfer and fluid flow during gas tungsten arc spot welding of low carbon steel. J Appl Phys 2003;93: 3022.

[38] Ren D, Liu L. Interface microstructure and mechanical properties of arc spot welding Mg–steel dissimilar joint with Cu interlayer. Mater Des 2014;59:369–76.

[39] Suzuki R, Ryo C. Aluminum-steel dissimilar robotic arc spot welding with auxiliary insert. Weld World 2019;63:1733–46.

[40] Wartelle A, Pouet B, Breugnot S. Industrial laser-ultrasonic receivers: recent progress in multichannel random-quadrature interferometers. Far East NDT Forum 2012:1–9.

[41] Imura F, Kita R, Nomura K, Asai S. Development of the in-situ measurement of the molten pool shape during TIG welding using laser ultrasonic. Q J Jpn Weld Soc 2018;36(1):49–59 [in Japanese)].